Space Object Detection in Images Using Matched Filter Bank and Bayesian Update

AE8900 MS Special Problems Report
Space Systems Design Lab (SSDL)
Guggenheim School of Aerospace Engineering
Georgia Institute of Technology
Atlanta, GA

Author:
Timothy S. Murphy

Advisor:
Marcus J. Holzinger

December 11, 2015

AE 8900 : Space Object Detection in Images Using Matched Filter Bank and Bayesian Update

Timothy S. Murphy [*] and Marcus J. Holzinger, [†]

Georgia Institute of Technology, Atlanta, GA, 30332

Brien Flewelling [‡]

Air Force Research Lab, Albuquerque, NM, 87116

Electro-optical sensors, when used to track space objects, are often used to produce detections for some orbit determination scheme. Instead, this paper proposes a series of methods to use electro-optical images directly in orbit determination. This work uses the SNR optimal image filter, called a matched filter, to search for partially known space objects. By defining a metric for measuring matched filter template similarity, a bank of matched filters is efficiently defined by partitioning the prior knowledge set. Once partitioned sets are known, the matched filter bank can be localized to regions of the sky. A method for hypothesis testing the result of a matched filter for a space object is developed. Finally, a framework for orbit determination based on the matched filter result is developed. Simulation shows that the analytic results enable a better framework for implementing matched filters for low SNR object detection.

Nomenclature

Spaces and Sets

$\mathbb{A}$	=	Space of Measurement arcs, $\mathcal{A}_m$
$\mathbb{R}$	=	Real Numbers
$\mathbb{Z}$	=	Integers
$\mathbf{SO}(2)$	=	Space of directions in $\mathbf{R}^3$
$\mathcal{A}_r$	=	Orbit arc
$\mathcal{A}_m$	=	Measurement arc
$\mathcal{O}_i$	=	Subset of $\mathbf{SO}(2)$ which observed by observer i
$\mathcal{S}$	=	Set of orbits
$\mathcal{S}_0$	=	Prior set of orbits
$\mathcal{S}_k$	=	Partition set of orbits
$\mathcal{T}$	=	Exposure time of sensor
$\mathpzc{AR}$	=	admissible region set representation

Matrices, Vectors, and Scalars

$\mathbf{Z}$	=	Measured image (ADU)
$\mathbf{M}$	=	Measured image signal content (ADU)
$\mathbf{W}$	=	Measured image noise content (ADU)
$\mathbf{M}_0$	=	Predicted image signal content (ADU)
$\mathbf{x}$	=	Space object state space representation
$\mathbf{r}$	=	Orbital position
$\mathbf{o}_i$	=	Position of observer i
$\boldsymbol{\rho}$	=	vector from observer to space object
$\mathbf{x}_u$	=	Undetermined states from a measurement
$\mathbf{x}_d$	=	Determined states from a measurement
$\mathbf{k}$	=	Observer parameters
i	=	denotes which observer is being considered
j	=	denotes which pixel in an image is being considered
z_j	=	Element of $\mathbf{Z}$ (ADU)
μ_j	=	Element of $\mathbf{M}$ (ADU)
w_j	=	Element of $\mathbf{W}$ (ADU)
n_z	=	Number of pixels which containing signal
$\Delta\theta$	=	angle between two vectors
d_{max}	=	Maximum threshold for the measurement dissimilarity metric
a_j	=	pixel values for a matched filter templates, $\mathbf{M}_0$
z_{MF}	=	result of a particular matched filter evaluation

Functions

g_{MF}	=	Matched filter function
$\mathbf{h}_i$	=	Instantaneous measurement function for observer i
$\tilde{\mathbf{h}}_i$	=	Pixel measurement function for observer i
ϕ	=	Flow function for orbital mechanics
d_{MDM}	=	Measurement dissimilarity metric (MDM)
f	=	Probability density function (PDF)

I. Introduction

The current Space Situation Awareness (SAA) problem involves, as part of it, the determination of a full description of the position and velocity of space objects (SO). The Space Surveillance Network (SSN) tracks upwards of 17,000 space objects of diameters greater than 10 cm. Small objects of diameter less than 10 cm which are not actively tracked still pose a threat to space assets [1]. Events like the Iridium-Cosmos collision highlight not only the possibility of future collisions but the potential for new space debris to be created [2]. It is predicted that similar high profile collisions will occur every 5 to 9 years [3]. Space and ground based electro-optical sensors (EOS) play a key role in tracking objects outside of Low Earth Orbit (LEO), where radar performance drops off. It can also be seen as an affordable alternative to radar technologies which tend to be costly [4]. Many of the small objects not already tracked by the SSN provide low strength optical signals, making detection by EOS difficult. In particular, the ability of an EOS to reliably detect a SO in a particular image is characterized by the Signal-to-Noise Ratio (SNR) defined as the ratio of the relevant signal strength to the standard deviation of the corrupting noise. Coder et. al. showed that lowering the algorithm-required SNR for image processing has the same sensitivity as lowering the the sensor-required signal strength [5]. Any research avenues which can allow sensors to effectively detect SO with lower SNR should be explored.

With prior information on an object, methods like rate tracking and matched filtering can enable lower SNR detections [6]. The matched filter (MF) is an image filter which provides a SNR gain, allowing information to be extracted from images with low SNR. Matched filtering originates in image and signal processing; the original formulation dates back to the 1960s as a way to detect a signal in a high noise environment [7]. It has been applied to a variety of relevant problems from dim asteroid detection to multi-frame moving target detection [8] [9]. A MF is based on a convolution of a known or hypothesized signal structure, called a template, with a measured image. Therefore, a MF requires a hypothesis or hypotheses on what signals should be expected. The most common way to generate a template is the velocity filter which linearizes the dynamics over an EOS exposure time for a particular hypothesis orbit [6]. If the underlying signal is unknown, a

brute force bank of velocity filters can be used [10]. The first problem with past use of the MF in SSA applications is the dynamics agnostic approach. The velocity filter linearization assumption is not always correct, especially when sensors contain significant rotation or distortion. The second, more relevant problem is prior knowledge is treated with a binary availability. Currently, a known space object is stored as a two line element (TLE). Many SO which either do not exist in the space object catalog or have not received updating measurements for long time periods may not be accurately described by their TLE or other prior information. There have been large pushes to properly model prior knowledge through methods like the admissible region and Gaussian mixture models [11] [12] [13]. These prior PDFs can be non zero over large ranges of orbital positions, implying any MF based on them should be a bank of plausible matched filters. This statistically rigorous framework can and should be the basis for hypothesis signals in a MF or MF bank. Work has also been done to incorporate hypothesis testing into SSA MFs, which will be included in this work [14].

While this paper focuses on matched filters as an SNR optimal technique, there are a multitude of methods for detecting and tracking low SNR space objects. Examples include multi-object filtering [15], multiple hypothesis testing [16], multi-frame matched filters [9], Track-Before-Detect, [17], Shift and add methods [18], and more. All of these methods, when applied to SSA images, rely on determining how an object moves through the sky around a certain observer. The work in this paper shows how to use partial orbit knowledge to generate hypothesized signals expected in images. While not explicitly explored in this paper, the hypotheses this paper formulates can be used as the basis for any of the above methods.

When considering an EOS attempting to measure a partially known object with low SNR, two problems are defined which are addressed in this paper. First, how can an EOS signal be predicted by partial orbit knowledge and how can that information be used to detect a SO? This paper approaches this problem by modeling a partially known SO as a set of possible orbits. The set of possible orbits is mapped into the frame of an EOS, providing a framework to rigorously search for an object. A metric will be used to partition this set and define a bank of matched filters [19]. Second, how can the results of this MF Bank be incorporated into the existing SSA framework? Methods involving hypothesis testing on matched filter results will be used to generate a likelihood function [14]. Then the likelihood will be applied in a Bayesian update formulation on the prior information, reformulated as a PDF, as a sequential particle filter. Another result which this paper will develop solves a problem with MF implementation for SSA. The MF is a discrete convolution of a known signal template with the measurement image. Traditionally, this is calculated over the entire image, but for SSA, the location of the SO is typically known. Large computation times can be saved if the MF is only calculated in certain localized areas. The framework which is developed for search for partially known SO easily allows for a localized matched filter search, which this paper will include.

The first contribution of this paper is the development of a matched filter based on true object dynamics. The second contribution of this paper is to define a metric which measures the similarity of EOS signals. The third contribution will be to introduce the SSA community to set partitioning based on metrics, and apply this theory to the matched filter bank. The fourth contribution will be to localize the matched filter bank to specific areas of an image based on partitioning. The fifth contribution will be show how matched filter results can be used as the measurement likelihood for a Bayesian update. The final contribution is the application of this framework to detect low SNR and dim space objects with an electro-optical sensor.

The paper organization is as follows. Section II introduces the concepts behind a MF which the reader should be familiarized with. Section III - A defines the problem set up and some of the functions this paper will use. Section III - B defines the framework for the partitioning process and the measurement dissimilarity metric. Section III - C develops a matched filter based partition for searching for partially known SO. Section III - D derives the measurement dissimilarity metric. Section III - E uses the measurement dissimilarity metric to develop an implementation for the partitioning process. Section III - F develops the localized matched filter process. Section IV gives intuition into how to implement this methodology. Section V simulated the

matched filter bank to demonstrate strengths. Appendix VI is included as a review of the basics of admissible regions theory.

II.   Matched Filter

This section reviews the concepts of matched filtering, image generation and processing, and mapping of continuous distributions to discrete images.

First, define a measurement as $\mathbf{Z}(t_0, t_I) \in \mathbb{Z}^{d_1 \times d_2}$ which is a matrix of pixel values, which are measured in analogue to digital units (ADU), for an EOS. Assume that the pixel z_j consist of some signal μ_j and zero mean Gaussian read noise w_j.

$$z_j = \mu_j + w_j \tag{1}$$
$$w_j \sim \mathcal{N}(0, \sigma_{w,j}) \tag{2}$$

Note that in this formulation, μ_j is equivalent to the mean of the measurement z_j. In order to have zero mean read noise in practice, an effective background subtraction method is needed [20]. The values t_0 and t_I represent the beginning time and length of the observer exposure, respectively. This allows the definition of the integration time set,

$$\mathcal{T} = [t_0, t_0 + t_I] \tag{3}$$

Each pixel is a integration of photons (or some unit of measure such as ADU) from a particular direction in the sky, and is therefore a function of the integration time set, $z_j(\mathcal{T})$. The matrix of pixels can be broken into signal and noise

$$\mathbf{Z}(\mathcal{T}) = \mathbf{M}(\mathcal{T}) + \mathbf{W}(\mathcal{T}) \tag{4}$$
$$\mathbf{M}(\mathcal{T}) \in \mathbb{Z}^{d_1 \times d_2}, \quad \mathbf{W}(\mathcal{T}) \in \mathbb{Z}^{d_1 \times d_2}$$

The pixel-wise SNR for a particular pixel, $z_j(\mathcal{T})$, in $\mathbf{Z}(\mathcal{T})$ for a fixed time interval is defined in Equation (5).

$$\begin{aligned} \mathrm{SNR}(z_j(\mathcal{T})) &= \frac{\mathbb{E}[z_j(\mathcal{T})]}{\sqrt{\mathbb{E}[(z_j(\mathcal{T}) - \mathbb{E}[z_j(\mathcal{T})])^2]}} \\ &= \frac{\mu_j(\mathcal{T})}{\sigma_{w,j}} \end{aligned} \tag{5}$$

Total object SNR is calculated as

$$\begin{aligned} \mathrm{SNR}\left(\sum z_j(\mathcal{T})\right) &= \frac{\mathbb{E}[\sum z_j(\mathcal{T})]}{\sqrt{\mathbb{E}[(z_j(\mathcal{T}) - \mathbb{E}[z_j(\mathcal{T})])^2]}} \\ &= \frac{\sum \mu_j(\mathcal{T})}{\sqrt{\sum \sigma_{w,j}^2}} \end{aligned} \tag{6}$$
$$\approx \sqrt{n_z} \frac{\bar{\mu}_j(\mathcal{T})}{\sigma_w} \tag{7}$$

where n_z is the number of pixels, $\bar{\mu}_j$ is the average signal value over the pixels being considered, and σ_w is some approximate per pixel noise. These SNR equations, Equation (7) in particular, rely on a simplification of noise properties in true images, and should only be taken as approximations. The MF is predicated on a hypothesized signal structure, which we will refer to as a template, $\mathbf{M}_0(\mathcal{T}) \in \mathbb{Z}^{d_3 \times d_4}$, which is a hypothesis of the signal contained in $\mathbf{M}(\mathcal{T})$. $\mathbf{M}_0(\mathcal{T})$ is a smaller or equal dimension matrix than $\mathbf{M}(\mathcal{T})$, that is $d_1 \geq d_3$ and $d_2 \geq d_4$ due to the constraint that the observed true signal cannot be larger than the entire optical frame. It should be noted that $\mathbf{M}_0(\mathcal{T})$ is not always a function of the exposure time, but could be predicated on any number of factors. For optical observation, the signal is dependent on the timing of the exposure making $\mathbf{M}_0(\mathcal{T})$ dependent on the timing of the exposure. A matched filter can then be defined as a mapping $g_{MF} : \mathbb{Z}^{d_1 \times d_2} \times \mathbb{Z}^{d_3 \times d_4} \rightarrow \mathbb{Z}^{d_1 \times d_2}$

$$\mathbf{Z}'(\mathcal{T}) = g_{MF}(\mathbf{Z}(\mathcal{T}), \mathbf{M}_0(\mathcal{T})) \tag{8}$$

The matched filter gives an optimal SNR gain for linear image filters [21] [22]. In other words, if the predicted signal $\mathbf{M}_0(\mathcal{T})$ is identical to the measured signal in $\mathbf{M}(\mathcal{T})$, the resulting SNR will be maximized. In practice, the function g_{MF} is a discrete convolution of $\mathbf{M}_0(\mathcal{T})$ centered on every pixel in $\mathbf{Z}(\mathcal{T})$. Although the words correlation and convolution are often used interchangeably, the calculation that is preformed is a convolution integral, while the resulting values are often referred to as the correlation between the template and signal. These results may be normalized to make perfect correlation positive one and perfect anti-correlation negative one.

III.   Theory

A.   Definition of Problem and Dynamics

This Subsection will present the background material for the paper. Consider a space object, with a state $\mathbf{x}(t)$ composed of position and velocity $\mathbf{r}(t)$ and $\dot{\mathbf{r}}(t)$, seen by an optical observer at position and velocity $\mathbf{o}(t)$ and $\dot{\mathbf{o}}(t)$ along line-of-sight vector, $\boldsymbol{\rho}(t)$. It should be noted that while this paper will assume $\mathbf{x}(t) \in \mathbb{R}^6$, as position and velocity, this can be generalized to any formulation of an orbit as well. The observer itself could be either ground based or space based. The geometry are illustrated in Figure 1.
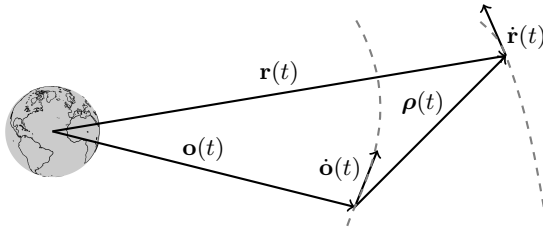

Figure 1. Geometry of general observer problem.

At an instantaneous time, an EOS measures a unit vector $\hat{\boldsymbol{\rho}}(t)$. This allows the following partition of the state

$$\mathbf{x}'(t) = \begin{bmatrix} \mathbf{x}_d^T(t) & \dot{\mathbf{x}}_d^T(t) & \mathbf{x}_u^T(t) \end{bmatrix}^T$$
$$\mathbf{x}_d(t) = \hat{\boldsymbol{\rho}}(t) \in \mathbf{SO}(2)$$
$$\dot{\mathbf{x}}_d(t) = \dot{\hat{\boldsymbol{\rho}}}(t) \in \mathbb{R}^2$$
$$\mathbf{x}_u(t) = [\rho(t) \;\; \dot{\rho}(t)]^T \in \mathbb{R}^+ \times \mathbb{R}$$

Note that $\boldsymbol{\rho} = \rho\hat{\boldsymbol{\rho}}$. As a reminder, $\mathbf{SO}(2)$ is the set of directions in $\mathbb{R}^3$. It can be represented by unit vectors and can also be thought of as the set of points that lie on the unit sphere or celestial sphere. It is easy to see that $\mathbf{x}'$ is simply a representation of $\mathbf{x} = [\mathbf{r}^T \;\; \mathbf{v}^T]^T$ in an observer-centric, spherical coordinate frame. Therefore, there exists a transformation between the two representations of the state

$$\mathbf{x}'(t) = \mathbf{m}(\mathbf{x}(t); \mathbf{k}_i(t)) \qquad (9)$$

where $\mathbf{k}_i(t)$ is a parameter vector containing $\mathbf{o}_i(t)$ and $\dot{\mathbf{o}}_i(t)$, observer i, and any other information needed on the observer. Multiple measurements or a non-zero exposure time allow inference of the rate of change of the unit vector, allowing the following further definition

$$\mathbf{x}_d'(t) = [\mathbf{x}_d^T(t) \;\; \dot{\mathbf{x}}_d^T(t)]^T \qquad (10)$$

In general, $\dot{\mathbf{x}}_d$ is inferred from two $\mathbf{x}_d$ measured at different times. It is useful to define the following instantaneous measurement function, which maps an orbit at a particular time to a measurement as seen by a particular observer, i.

$$\mathbf{x}_d(t) = \mathbf{h}_i(\mathbf{x}(t); \mathbf{k}_i(t)) \qquad (11)$$

This paper works heavily with sets of orbits which will be mapped to a particular EOS measurement space.. In general, if $\mathcal{S}$ is a set of orbits at time t, then

$$\mathcal{S}_i(t) = \mathbf{h}_i(\mathcal{S}(t); \mathbf{k}_i(t)) \qquad (12)$$

gives these orbits mapped into points in $\mathbf{SO}(2)$, centered around $\mathbf{o}_i$. For ease of notation, the parameter vector $\mathbf{k}$ may be dropped from Equation (11), but is always implied.

Matched filtering relies on predicting the image that an optical observer will produce based on the presence of a particular SO. The actual measurement obtained is the integration of a time-varying line-of-sight unit vector, $\hat{\boldsymbol{\rho}}(t)$, over an exposure time $t \in \mathcal{T} = [t_0, t_0 + t_I]$. Each bin on the CCD obtains photons from a small subset of $\mathbf{SO}(2)$. As the line-of-sight vector $\hat{\boldsymbol{\rho}}(t)$ changes over the exposure, it illuminates different pixels, producing an image that the user sees. This process, which can be seen in Figure 2, is defined as the mapping

$$\mathbf{M}(\mathcal{T}) = \tilde{\mathbf{h}}_i(\mathbf{x}_d'(t); \mathcal{T}, \mathbf{k}_i(t)) \qquad (13)$$

which represents the model for a particular observer's mapping from angular space into pixel values. This transformation may include further observer parameters which are also contained in the observer parameter vector, k_i.
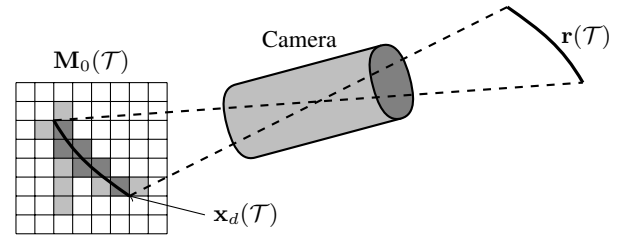

Figure 2. Modeling an optical observer in Equation (13).

The prediction of objects also requires modeling the movement of objects through space. This paper will use the flow function to map $\mathbf{x}(t)$ through time.

$$\mathbf{x}(t) = \boldsymbol{\phi}(t; \mathbf{x}(t_0), t_0) \qquad (14)$$

For a typical SO this is practically done by integrating the nonlinear dynamics with a differential equation solver.

The admissible region (AR) will be used throughout this paper as an example to illustrate parts of the discussion. A review of admissible region theory in shown in Appendix VI. When an AR is represented as a set, the notation $\mathscr{A\!R}$ will be used.

B.   General Matched Filter Primed by Previous Orbital Knowledge

The first contribution of this paper is proposing a MF for orbital tracking applications that does not require a constant velocity assumption. Assume there exists a hypothesis orbit of a SO, $x(t_0)$. This hypothesis can then be mapped to the measurement frame of an observer i via Equation (11). This hypothesis can also be mapped forward in time using the known flow function from Equation (14).

$$\mathbf{x}_d(t) = \mathbf{h}_i(\boldsymbol{\phi}(t; \mathbf{x}(t_0), t_0), \mathbf{k}_i(t)) \qquad (15)$$

In reality, the result of interest is to predict the object's trajectory over a known integration time. By varying t, a hypothesized orbit, $\mathbf{x}(t)$, can be mapped to any point in the integration time of an observer. This hypothesis can then be used to calculate the orbit arc $\mathcal{A}_r$ through $\mathbb{R}^3 \times \mathcal{T}$,

$$\mathcal{A}_r = \{[\mathbf{r}^T(t), t]^T \in \mathbb{R}^3 \times \mathbb{R} :$$
$$\mathbf{r}(t) = [I_{3\times3} \;\; 0_{3\times3}] \; \boldsymbol{\phi}(t; \mathbf{x}(t_0), t_0), t \in \mathcal{T}\} \qquad (16)$$

This is simply the trajectory of the orbit over the integration time, with associated time history. $\mathcal{A}_r$ is labeled in Figure 3. In reality, an optical observer does not observe the true arc of the orbit, but rather the

arc through angular space, or $\mathbf{SO}(2)$. Similarly, $\mathcal{A}_m$ can be defined as an arc through $\mathbf{SO}(2)$ in Equation (17).

$$\begin{aligned} \mathcal{A}_m = \{[\mathbf{x}_d^T(t), t]^T \in \mathbf{SO}(2) \times \mathbb{R} : \\ \mathbf{x}_d(t) = \mathbf{h}_i(\boldsymbol{\phi}(t; \mathbf{x}(t_0), t_0), \mathbf{k}(t)), t \in \mathcal{T}\} \end{aligned} \quad (17)$$

This measurement arc is the arc $\mathcal{A}_r$ mapped through Equation (11). The measurement arc and this mapping process can be visualized in Figure 3. $\mathbf{SO}(2)$ is represented by a unit sphere. While the notation of mapping $\mathcal{A}_r$ to $\mathcal{A}_m$ is useful for visualization purposes, the ultimate purpose of this discussion is to map an orbit to a measurement arc. The following mapping is defined

$$\mathcal{A}_m = \mathbf{h}_i(\mathbf{x}(t); \mathcal{T}) \quad (18)$$

which maps an orbit, $\mathbf{x}(t)$, with an associated integration time, $\mathcal{T}$, to a measurement arc, $\mathcal{A}_m$. The use of $\mathbf{h}_i$ is a slight abuse of notation; it is assumed that the orbit is integrated over the exposure time to allow this new mapping. It is assumed that when $\mathbf{h}_i$ is used, time history is preserved alongside the position history. The time history will be needed in Subsection D.
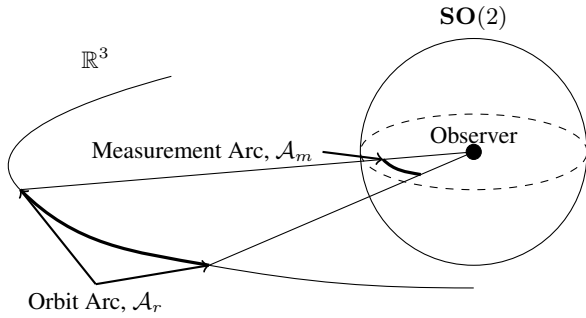

Figure 3. Mapping of orbit to measurement arc.

In addition, the measurement arc will ultimately be mapped to a template which exists as predicted EOS pixel values so Equation (13) should be redefined as

$$\mathbf{M}(\mathcal{T}) = \tilde{\mathbf{h}}_i(\mathcal{A}_m, \mathbf{k}_i) \quad (19)$$

In practice, $\mathcal{A}_m$ should be discretized over the integration time, and each discrete point mapped into a pixel. It is also worth noting that $\mathcal{A}_m$ is sensor specific. Perhaps a better notation would be $\mathcal{A}_{m,i}$, where i denotes the sensor. It should be clear which sensor is being considered throughout this paper, so the i notation will be omitted. Modeling phenomenology such as atmospheric blurring and distortion models is advisable but not required. This MF template is built directly from the hypothesized SO signal structure, accounting for observer motion, and has no built in linearization.

Equation (18) represents the culmination of the results in this subsection. This measurement arc, $\mathcal{A}_m$ is a mathematically rigorous equivalent to the measurement an observer would take. This subsection lays down a framework for creating templates based on orbits. The final result is an image that models what an EOS should see. In general, there are more considerations that should be included in template generation. This can include but is not limited to SO apparent brightness and subpixel localization. These processes will be discussed in Section IV.

This paper will discuss sets of measurement arcs. Typically, these will result from mapping sets of orbits through Equation (17). This paper will therefore define $\mathbb{A}$ for a given t_0, t_I as the set of all possible measurement arcs.

$$\mathbb{A} = \{\mathcal{A}_m = \mathbf{h}_i(\mathbf{x}, t_0, t_I) : \mathbf{x} \in \mathbb{R}^6\} \quad (20)$$

This is convenient for defining subsets of $\mathbb{A}$ in Subsection D.

C. Matched Filter Bank Primed by Prior Distribution

This subsection will motivate the need for a bank of matched filters, provide an explanation for how partitions can correctly define a bank of matched filters, and finalize the definition of this partitioning. It should be noted that, without loss of generality, a single observer is being consider from here on, so the i notation will be dropped.

Consider prior information in the form of a set of orbits, $\mathcal{S}_0$, which is referred to as the prior set. By creating s non-overlapping subsets which cover $\mathcal{S}_0$, a partitioning can be created for the prior set.

$$\mathcal{S}_0 = \bigcup_{k=1}^s \mathcal{S}_k \quad (21)$$

$$\mathcal{S}_l \cap \mathcal{S}_k = \emptyset, \forall l \neq k \quad (22)$$

It is not necessary that the partitioning be non-overlapping, and certain partitioning schemes may benefit from this condition being relaxed. The intention is to define each partition set, $\mathcal{S}_k$, such that all orbits from this set produce templates nearly identical to some representative template, $\mathbf{M}_k$.

$$\mathcal{S}_k = \{\mathbf{x}(t) : \mathbf{M}_k \approx \tilde{\mathbf{h}}(\mathbf{h}(\mathbf{x}(t); \mathcal{T}, \mathbf{k}))\} \quad (23)$$

It is generally the case that a single subset set $\mathcal{S}_k \subseteq \mathcal{S}_0$ will not contain all possible orbits from a prior distribution implying a series of sets, $\{\mathcal{S}_k\}_{k=1}^{k=s}$. This is the basis on which a bank of matched filters will be defined.

Next, an analysis of the contents of $\mathcal{S}_k$ will be presented. Consider a nominal orbit, $\bar{\mathbf{x}}$, and its particular measurement arc, $\bar{\mathcal{A}}_m$, with arbitrary time and observer parameters.

$$\bar{\mathcal{A}}_m = \mathbf{h}(\bar{\mathbf{x}}(t); \mathcal{T}) \quad (24)$$

The measurement mapping defined in Equation (11) maps a position in $\mathbb{R}^3$ to the two dimensional space $\mathbf{SO}(2)$ through the equation

$$\boldsymbol{\rho} = \mathbf{r} - \mathbf{o} \quad (25)$$

$$\hat{\boldsymbol{\rho}} = \frac{\boldsymbol{\rho}}{\|\boldsymbol{\rho}\|} \quad (26)$$

where $\| \cdot \|$ is the 2-norm. Note that while $\hat{\boldsymbol{\rho}}$ is vector in $\mathbf{R}^3$, it only has two free dimensions as an element of $\mathbf{SO}(2)$. Because this is the mapping on which the measurement arc is based, different $\boldsymbol{\rho}$ inputs which vary only in magnitude will all map to a single $\hat{\boldsymbol{\rho}}$. Therefore there must exist a non-trivial set of orbits, $\bar{\mathcal{S}}$, with corresponding orbit arcs which all map to the same measurement arc.

$$\bar{\mathcal{S}} = \{\mathbf{x} \in \mathbb{R}^6 : \bar{\mathcal{A}}_m = \mathbf{h}(\mathbf{x}(t); \mathcal{T})\} \quad (27)$$

This is an inversion of the admissible region argument; instead of having a measurement and creating a set of consistent orbits, consistent orbits are being grouped together to predict a measurement. A single partition, defined in this way, is illustrated in Figure 4. Small enough variations in $\bar{\mathcal{A}}_m$ will provide effectively identical templates. In order to have an effective matched filter, the template does not necessarily need to be perfect; it may benefit a user to have less templates with an increased risk of imperfect matching but decreased computation time. It is possible to define a new partition set:

$$\mathcal{S}_k = \{\mathbf{x} \in \mathcal{S}_0 : d(\bar{\mathcal{A}}_m, \mathbf{h}(\mathbf{x}(t); \mathcal{T})) \leq d_{max}\} \quad (28)$$

where $d : \mathbb{A} \times \mathbb{A} \to \mathbb{R}^+$ defines a metric which evaluates the difference between two measurement arcs. Assuming an appropriate metric exists, all orbits in $\mathcal{S}_k$ produce measurement arcs similar enough to $\bar{\mathcal{A}}_m$.

Prior knowledge is often some probability density function (PDF), available from an a posteriori estimate. In the extreme case of object discovery, this PDF may be large, consisting of an admissible region, or a large Gaussian mixture or discrete particle distribution. For this

analysis, it is necessary to define a prior set of orbits, $\mathcal{S}_0$. In the case of a PDF, this could be thought of as the interior of an iso-probability surface of the PDF which is used to create this prior set, $\mathcal{S}_0$

$$\mathcal{S}_0 \triangleq \{\mathbf{x} \in \mathbb{R}^6 : f(\mathbf{x}) > f_{min}\} \tag{29}$$

where the function $f : \mathbb{R}^6 \to \mathbb{R}^+$ is the prior PDF over the state space.
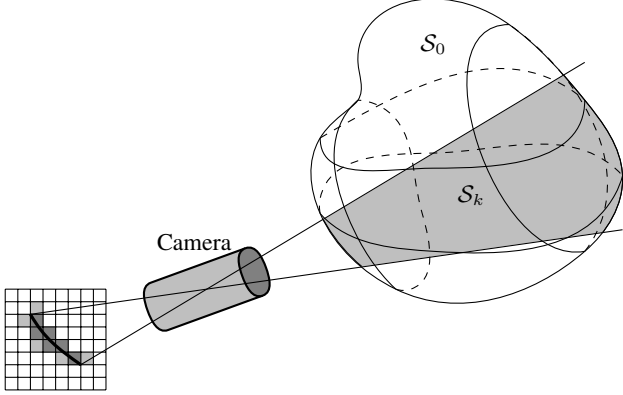
The next subsection will go on to define a suitable metric, d, for Equation 28.

Figure 4. A non trivial region of orbits will all map to a single MF template.

D. Measurement Dissimilarity Metric

A bank of MF are desirable for large prior distributions, but due to computation time it is also useful to choose a minimal number of templates. This subsection is concerned with creating a framework to allow similar templates to be grouped together. Conversely, templates which are sufficiently different in shape should not be grouped together. Therefore, a measure of similarity of templates is necessary. As it has been shown before, the measurement arc A_m defined in Equation (17) is a mathematical equivalent to the MF template, $\mathbf{M}_0(t)$. There could be many ways to compare similarity of measurement arcs, but a metric has many desirable properties. The most important feature of metrics which motivates this discussion is the existence of a large body of work on partitioning metric spaces. Previous work on partitioning metric spaces will be discussed in Subsection E, after the metric to be used has been defined [19].

The first step is to choose an existing metric to compare arc similarity. First, consider the similarity of two points on the celestial sphere, $\hat{\boldsymbol{\rho}}_a(t)$ and $\hat{\boldsymbol{\rho}}_b(t)$. The distance between points on the surface of a sphere, along the surface of the sphere, is called the great-circle distance or orthodromic distance and is defined as:

$$\Delta\theta_{a,b}(t) = 2\sin^{-1}\left(\frac{||\hat{\boldsymbol{\rho}}_a(t) - \hat{\boldsymbol{\rho}}_b(t)||}{2}\right) \tag{30}$$

This particular formulation of the orthodromic distance assumes $\hat{\boldsymbol{\rho}}_a(t)$, $\hat{\boldsymbol{\rho}}_b(t)$ are both unit vectors. The unit vector assumption makes orthodromic distance equivalent to the angle between the unit vectors, in radians. A metric which compares two measurement arcs is desirable. When considering the entire measurement arc, integrating $\Delta\theta_{a,b}(t)$ over a predefined exposure time, $[t_0, t_0 + t_I]$ takes into account how two measurement arcs differ over the relevant time interval. Thus the measurement dissimilarity metric (MDM) for a given $[t_0, t_0 + t_I]$ is defined in Equation (31).

$$d_{MDM}(\hat{\boldsymbol{\rho}}_a(t), \hat{\boldsymbol{\rho}}_b(t)) = \int_{t_0}^{t_0+t_I} \Delta\theta_{a,b}(\tau)d\tau \tag{31}$$

This metric can be wrapped into the measurement arc notation defined in Subsection B. Given a particular measurement arc, $\mathcal{A}_{m,a}$, defines a time-varying unit vector, $\hat{\boldsymbol{\rho}}_a(t)$ over a predefined time interval $[t_0, t_0 + t_I]$. Therefore, the MDM can be directly computed between two measurement arcs.

$$d_{MDM}(\mathcal{A}_{m,a}, \mathcal{A}_{m,b}) = \int_{t_0}^{t_0+t_I} \Delta\theta_{a,b}(\tau)d\tau \tag{32}$$

Lemma III.1. *The measurement dissimilarity metric defined in Equation* (32) *over a fixed time interval,* $[t_0, t_0 + t_I]$*, is a metric on* $\mathbb{A}$*, the set of measurement arcs, for any pair* $\hat{\boldsymbol{\rho}}_a(t) \in \mathcal{A}_{m,a}, \hat{\boldsymbol{\rho}}_b(t) \in \mathcal{A}_{m,b}$*, that is, it satisfies the following:*

1. $d_{MDM}(\mathcal{A}_{m,a}, \mathcal{A}_{m,b}) \geq 0$ (non-negativity)

2. $d_{MDM}(\mathcal{A}_{m,a}, \mathcal{A}_{m,b}) = 0$ *if and only if* $\hat{\boldsymbol{\rho}}_a(t) = \hat{\boldsymbol{\rho}}_b(t)$ (coincidence)

3. $d_{MDM}(\mathcal{A}_{m,a}, \mathcal{A}_{m,b}) = d_{MDM}(\mathcal{A}_{m,b}, \mathcal{A}_{m,a})$ (symmetry)

4. $d_{MDM}(\mathcal{A}_{m,a}, \mathcal{A}_{m,c}) \leq d_{MDM}(\mathcal{A}_{m,a}, \mathcal{A}_{m,b}) + d_{MDM}(\mathcal{A}_{m,b}, \mathcal{A}_{m,c})$ (triangle inequality)

Proof. Non negativity follows directly from the range of the functions involved.

$$||\hat{\boldsymbol{\rho}}_a - \hat{\boldsymbol{\rho}}_b|| \in [0, 2]$$
$$\sin^{-1}\left(\frac{||\hat{\boldsymbol{\rho}}_a(t) - \hat{\boldsymbol{\rho}}_b(t)||}{2}\right) \in [0, \pi/2]$$
$$\Delta\theta_{a,b}(t) \geq 0$$
$$\int_{t_0}^{t_0+t_I} \Delta\theta_{a,b}(t)dt \geq 0 \tag{33}$$

For coincidence, first note that $\int_{t_1}^{t_2} f(t)dt = 0 \iff f(t) = 0, \forall t \in [t_1, t_2]$, for any continuous function $f(t)$ and arbitrary values of t_1 and t_2. Next, note that over the range of inputs, $x \in [0, 1], \sin^{-1}(x) = 0 \iff x = 0$. This directly implies 2. This is equivalent to saying the only way the measurement dissimilarity metric can be zero is if the measurement arcs are identical.

For symmetry, note that $||\hat{\boldsymbol{\rho}}_a - \hat{\boldsymbol{\rho}}_b|| = ||\hat{\boldsymbol{\rho}}_b - \hat{\boldsymbol{\rho}}_a||$ for an arbitrary pair of unit vectors. 3 follows immediately.

The shortest distance along the surface of a sphere between two points is the orthodromic distance. Therefore $\Delta\theta_{a,c}(t) \leq \Delta\theta_{a,b}(t) + \Delta\theta_{b,c}(t)$ must be true, because $\Delta\theta_{a,b}(t) + \Delta\theta_{b,c}(t)$ represents another path along the surface of a sphere from a to c. Remember the following property of integrals

$$f_a(t) \leq f_b(t) \Rightarrow \int_{t_1}^{t_2} f_a(t)dt \leq \int_{t_1}^{t_2} f_b(t)dt$$

which is true for any t_1 and t_2.

$$\int_{t_0}^{t_0+t_I} \Delta\theta_{a,c}(t)dt \leq \int_{t_0}^{t_0+t_I} \Delta\theta_{a,b}(t)dt + \int_{t_0}^{t_0+t_I} \Delta\theta_{b,c}(t)dt \tag{34}$$

This gives the triangle inequality. □

Thus, the MDM is a metric on $\mathbb{A}$, the set of measurement arcs, allowing partition methods to be applied to $\mathbb{A}$. The desired partitioning will, however, be occurring on orbits which exist as elements in $\mathbb{R}^6$. The MDM can also be defined over a set of orbits because of the onto mapping from orbits to measurement arcs, Equation (18). This can also be shown by acknowledging that $\hat{\boldsymbol{\rho}}_a(t)$ is a function of $\mathbf{x}(t)$.

$$\Delta\theta_{a,b}(t) = 2\sin^{-1}\left(\frac{||\hat{\boldsymbol{\rho}}_a(\mathbf{x}(t)) - \hat{\boldsymbol{\rho}}_b(\mathbf{x}(t))||}{2}\right)$$

$$d_{MDM}(\mathbf{x}_a, \mathbf{x}_b) = \int_{t_0}^{t_0+t_I} \Delta\theta_{a,b}(\tau)d\tau \qquad (35)$$

The following corollary will show that the MDM is a pseudo-metric on $\mathbb{R}^6$, or any set of orbits.

Corollary III.2. *The measurement dissimilarity metric defined in Equation* (31) *over a fixed time interval, $t \in [t_0, t_0 + t_I]$, is a pseudo-metric on $\mathbb{R}^6 \times \mathbb{R}$ for any pair of orbits $\mathbf{x}_a(t), \mathbf{x}_b(t)$, that is, it satisfies the following:*

1. $d_{MDM}(\mathbf{x}_a(t), \mathbf{x}_b(t)) \geq 0$ (non - negativity)
2. $d_{MDM}(\mathbf{x}_a(t), \mathbf{x}_b(t)) = d_{MDM}(\mathbf{x}_b(t), \mathbf{x}_a(t))$ (symmetry)
3. $d_{MDM}(\mathbf{x}_a(t), \mathbf{x}_c(t)) \leq d_{MDM}(\mathbf{x}_a(t), \mathbf{x}_b(t)) + d_{MDM}(\mathbf{x}_b(t), \mathbf{x}_c(t))$ (triangle inequality)

Proof. Non negativity and symmetry follow from Lemma III.1. Every orbit will map to a measurement arc which exists on $\mathbb{A}$.

First fix three orbits, $\mathbf{x}_a$, $\mathbf{x}_b$, and $\mathbf{x}_c$. Because the mapping from orbits to measurement arcs is onto, these orbits map to single time-varying unit vectors, $\hat{\boldsymbol{\rho}}_a(t)$, $\hat{\boldsymbol{\rho}}_b(t)$, and $\hat{\boldsymbol{\rho}}_c(t)$. The triangle inequality follows from Lemma III.1. □

The pseudo-metric does not have a coincidence property because the mapping from orbits to measurement arcs is not one-to-one. However, Subsection E will discuss metrics rather than psuedo-metrics. In order to enable metric space partitioning based on pseudo-metrics, co-incident objects are considered as one object [23]. This is equivalent to saying all orbits that produce the identically same streak are the same object. Such a simplification is the inversion of the admissible region argument. Instead of having a measurement and creating a set of consistent orbits, consistent orbits are being grouped together to predict a measurement. Each $\mathscr{R}$ is an individual object in the space to be partitioned. This definition is a mathematical necessity, but does not change the partition process in the next subsection. A prior set could be redefined by grouping admissible regions analytically, but such an analysis is unnecessary and not included in this paper.

One question remains: is the MDM robust to the presence of sensor dynamics and distortion? If a sensor is rotating, all objects in a measurement frame appear to arc and rotate through the measurement frame. Furthermore, this rotation can be different depending on where an object is in the sensor frame. Sensor distortion can alter streaks as a function of where they occur in the frame. Different templates will then be needed for different localized areas. Equation (19) includes an assumed dependence on $\mathbf{k}$, the parameter vector which includes $\mathbf{o}, \dot{\mathbf{o}}$. The parameter vector can be expanded to include parameters on local sensor distortion and observer rotation to address this. For typical distortion and rotation models, the number of distinct templates should be minimal The error produced by not including a correct should be small for most narrow field of view sensors. The localization analysis in Subsection F should further reduce this problem. An in-depth analysis of these effects and how best to localize them is out of the scope of this paper.

E.   Metric-Based Partitioning

The properties of a metric seem obvious and trivial at first glance, but in fact a wide variety of partition methods exist. A good discussion of metric-based search and partition methods can be found in the text *Similarity Search: The Metric Space Approach* by Zezula et al. [19]. An overview of the concepts and methods will be discussed here. The broad approach falls into two categories, ball partition (BP) methods and generalized hyperplane tree (GHT) methods [24] [23]. The literature is rich with implementations of these methods. Most variations of methods are attempts to improve methods for particular situations or overcoming general pitfalls. The bulk of these methods are simply a reworked BP or GHT method. This subsection will aim to introduce the field of metric-based partitioning.

BP is the first method and is based around a predetermined maximum distance, d_{max}. It can be visualized in Figure 5a. First, a maximum dissimilarity of two measurements, d_{max}, is defined as sufficient difference for templates to be unique. Once a d_{max} is set, BP is straightforward. BP is implemented by choosing a series of pivot points, $x_k \in \mathcal{S}_0$. Each partition $\mathcal{S}_a$ is a ball centered at a respective pivot, x_a, with a radius d_{max}

$$\mathcal{S}_k = \{x \in \mathcal{S}_0 : d_{MDM}(x, x_k) \leq d_{max}\} \qquad (36)$$

It should be noted that BP typically violates, Equation 22, that is the partitions overlap each other. This does not change the end result of the algorithm, so it is nothing more than a mathematical observation. The second method is analogous to the Voronoi diagram. It can be visualized in Figure 5b. The generalized hyperplane tree (GHT) is implemented by setting a number of pivots and then binning the rest of the space by defining hyperplanes of equal metric distance from each pair of pivots. Each partition is then the set of points which are closer to a particular pivot than any other pivot.

$$\mathcal{S}_k = \{x \in \mathcal{S}_0 : d_{MDM}(x, x_k) \leq d_{MDM}(x, x_l)\} \qquad (37)$$

In practice, the set is represented as a discrete point-wise approximation and the points are sorted. This can be done as a single run, with a large number of pivots, or recursively, gradually adding pivot points.
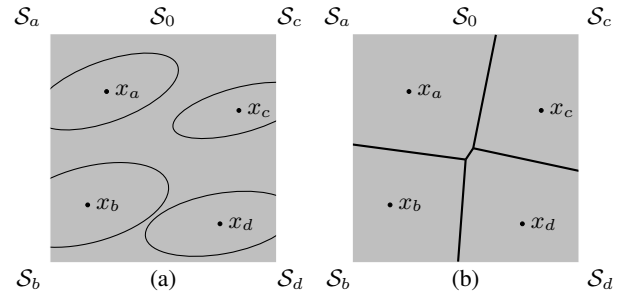

Figure 5. Ball partition and generalized hyperplane methods [19]

The hyperplanes can be calculated analytically in theory, but in practice this is difficult. An easier approach to this may be to calculate a Taylor series expansion of the MDM around all desired pivot points. This allows the hyperplanes to be approximated, but has all the problems that come with linearization. If discrete partitioning becomes computationally costly, this may be a solution. Computation of this expansion is out of the scope of this paper.

In this process, a few questions still exist: what should d_{max} be set as and why, and how fine does the discrete point-wise approximation need to be?

A higher value of d_{max} will result in fewer partitions, while a lower d_{max} will give more partitions. The accuracy of the templates will be dependent on how large the chosen d_{max} is. The computation time will be directly proportional to the number of templates chosen as well. Therefore, a "best" d_{max} is difficult to define and will be problem dependent.

A proposed way is to assure that the two measurements with $d_{MDM} \leq d_{max}$ appear essentially the same to an observer. Therefore, d_{max} should be based on the pixel size of the sensor s_x, the exposure time, t_{exp}, and length of the measurement arc L. The MDM as derived gives arc dissimilarity integrated over a time period. This gives weight to higher exposure times, which is is undesirable, so normalization by exposure time is necessary. $d_{MDM}(\hat{\boldsymbol{\rho}}_1(t), \hat{\boldsymbol{\rho}}_2(t))/t_{exp}$ is the average difference between two measurements, and is independent of exposure time. If this value were equal to the pixel size of the sensor, on average each pixel will have an error equal to one pixel. With long streaks over, 100 pixels, this could be a one pixel error everywhere or a ten pixel error over a tenth of the streak. What is desirable is that, at most, a single pixel has an error of one pixel.

$$d_{MDM}(\hat{\boldsymbol{\rho}}_1(t), \hat{\boldsymbol{\rho}}_2(t))/t_{exp} < \frac{s_x}{L} \tag{38}$$

L is the number of the pixels in the streak and allows d_{max} to be normalized for larger or smaller length streaks. If L varies from template to template, the maximum possible streak length should be used. This value in practice is very restrictive, and for this reason has not be implemented in the simulation results section. More analysis on how to analytically define a threshold for this process is needed.

The methods described thus far rely on a discrete point-wise approximation. As with any such approximation, sufficient particles are needed to allow the approximation to be representative of the set. This implies highly dimensional sets will be difficult to model. Exploiting sub-spaces of lower dimensionality is recommended, such as admissible regions. Insufficient particles can also lead to poorly defined partition set boundaries.

There are a wealth of specific implementation methods for BP, GHT, and more methods in the literature [25], [26]. This paper aims to introduce the concepts of similarity search as a way to solve problems in set-based SSA applications. For the simulations and results produced for this paper, a simple ball partitioning method was implemented. As the algorithms proposed in this paper mature, more work will be required to evaluate more optimal strategies for partitioning.

F. Localized Matched Filtering

The matched filter involves a discrete convolution of the template over the measurement image. The matched filter can be applied over the entire measurement image, but is a computationally costly process. If certain templates can be skipped or searched in only a local area, large computation times are saved. This subsection will define a method by which the partition sets can be used to localize the matched filter search.

When a particular hypothesis orbit is mapped into the sensor frame, $\mathcal{A}_m$ has an associated location in that frame. Each partition $\mathcal{S}_k$, as defined, is a set of hypothesis orbits. If a particular anchor time, t^*, is defined a particular partition can be mapped into $\mathbf{SO}(2)$.

$$\mathcal{S}'_k = \{\mathbf{x}_d \in \mathbf{SO}(2) : \mathbf{x}_d = \mathbf{h}(\phi(t^*; t_0, \mathbf{x}(t_0)), \mathbf{k}(t_0)), \mathbf{x}(t_0) \in \mathcal{S}_k, \} \tag{39}$$

For this particular partition's template to be necessary, the observer must be looking at the object during the exposure time.

$$\mathcal{O}_i = \{\mathbf{x}_d \in \mathbf{SO}(2) : \mathbf{x}_d \text{ in observer frame at } t^*\} \tag{40}$$

When a MF template is used to search an image, it is tiled over the pixels. This is done by choosing an anchor pixel in the template, typically the center pixel. This anchor pixel is aligned with each pixel in the image and then the convolution is evaluated. $\mathcal{S}'_k$ is the set of all unit vectors which can be generated from the partition set $\mathcal{S}_k$ at t^*. If the anchor pixel is defined as the location of the object at t^*, a search space can be defined

$$\mathcal{S}_{k,i} = \mathcal{O}_i \cap \mathcal{S}'_k \tag{41}$$

$\mathcal{S}_{k,i}$ represents the search space for template k in an image taken by observer i. This can be seen in Figure 6, where each template has local areas where it should be evaluated.

This method will yield one of two results. First, $\mathcal{S}_{k,i}$ can be empty, in which case the template does not require searching for a particular image. Second, $\mathcal{S}_{k,i}$ is non-empty, and the template need only be searched over a subset of $\mathcal{O}_i$. More generally, this illustrates a fundamental problem of searching for partially known SO: the search space defined by prior knowledge can be larger than what can be captured by a single measurement. The prior set, $\mathcal{S}_0$, and the subsets, $\mathcal{S}'_k$ can inform sensor tasking. For example, a tasking scheme could be to take a minimum number of observations to observe the entire set, $\mathcal{S}_0$. Tasking schemes for observing partially known space objects based on this framework is considered future work. Sensor pointing and orientation must be known in order to implement this method. In the case
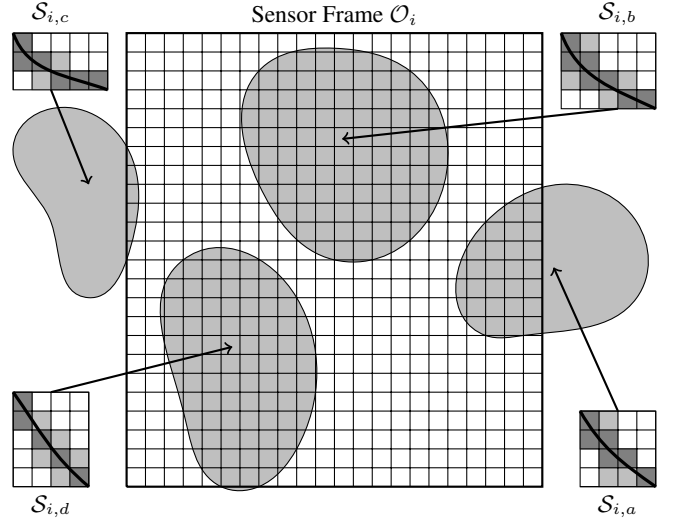

Figure 6. Localized searching of the sensor frame for partitions a through d

of significant uncertainty in pointing, search areas should be expanded appropriately (e.g. one pixel of point uncertainty implies one pixel of padding on search spaces is needed).

G. Probability of Detection and Likelihood Map from Matched Filter

Hypothesis testing on matched filter results is not a new concept [14]. Multiple methods exist and this paper makes no claims about which is best or worst. Instead, this subsection will present one possible formulation.

Consider a matched filter template which consists of n non-zero pixels a_j. When calculating the matched filter for a particular position, each pixel in the template is associated with a particular measurement pixel, z_j. Then the matched filter correlation is calculated by

$$z_{MF} = \sum_{j=1}^{n} a_j z_j \tag{42}$$

As per Section II, assume that the pixels consist of some signal, μ_j, and zero mean i.i.d. Gaussian read noise, w_j, shown in Equations (1) and (2). Note that in this formulation, μ_j is equivalent to the mean of the measurement z_j. In order to have zero mean read noise in practice, an effective background subtraction method is needed to remove artifacts including dark current and hot pixels. Under these assumptions, z_{MF} is distributed as follows:

$$\mathbb{E}[z_{MF}] = \sum_{j=1}^{n} a_j \mu_j$$

$$\text{Var}[z_{MF}] = \mathbb{E}\left[\left(\sum_{j=1}^{n} a_j w_j\right)^2\right] = \sigma_w \sum_{j=1}^{n} a_j^2$$

$$z_{MF} \sim \mathcal{N}(\Sigma \mu_j, \alpha \sigma_w) \tag{43}$$

where α is a scaling factor dependent on the actual weights, a_j. A hypothesis test is desired for determining if there is signal present which is effecting z_{MF}. This equivalent to asking if z_{MF} has a mean of zero or a mean greater than zero. Consider the null and test hypotheses for a binary hypothesis test, for a matched filter

$$H_0 : z_{MF} \sim \mathcal{N}(0, \alpha \sigma_w)$$
$$H_1 : z_{MF} \sim \mathcal{N}(\beta, \alpha \sigma_w), \ \ \beta > 0 \tag{44}$$

For binary hypothesis testing, a probability of false alarm is set, p_{FA}, which in term defines an integration threshold, z_{TH}, based on the null hypothesis PDF, $f_0(z)$.

$$p_{FA} = \int_{z_{TH}}^{\infty} f_0(z)dz \qquad (45)$$

The test hypothesis PDF, $f_1(z)$, is then integrated over, giving a probability of detection.

$$p_{Detect} = \int_{z_{TH}}^{\infty} f_1(z)dz \qquad (46)$$

For more on this subject, see [27]. This hypothesis test can be used to determine if there is significant evidence that the predicted signal exists in the predicted location. Because the matched filter gives an optimal SNR gain, this test should maximize p_{Detect}, though an explicit proof of this claim is out of the scope of this paper.

H. Orbit Determination and Sequential Bayesian Filter

The main motivating case for this research is an admissible region hand off for fast and accurate orbit determination. The basic case of this is trivial; if two observers with geometrically diverse locations observe a SO, the exact position can be triangulated [28]. For the case of observers at different times and positions attempting to perform orbit determination on a particular space object, more analysis is needed. First, consider the aforementioned matched filter bank, preformed on an admissible region detected by observer i, $Æ_i$. This admissible region can be propagated forward to time t_0, forming $\mathcal{S}_0$ and mapped into the sensor frame of a second observer j. If a statistically significant detection is made by the matched filter bank, a measurement can be made. This measurement, made by observer j, will consist of the determinable states for an EOS:

$$\mathbf{x}'_{d,j}(t_0) = [\alpha(t_0), \delta(t_0), \dot{\alpha}(t_0), \dot{\delta}(t_0)]^T \qquad (47)$$

If the calculated $\mathbf{x}'_{d,j}(t_0)$ is not consistent with the location and rate of the template used to detect it, then the measurement can be disregarded; the object that has been detected is not consistent with any hypothesis generated from $\mathcal{S}_0$. Assuming, the measurement and template are consistent, an admissible region, $Æ_j$, can be constructed. Now, there exists two sets $\mathcal{S}_0$ and $Æ_j$ both represented by orbits at a particular time, t_0. Furthermore, it is known that both admissible regions contain an orbit consistent with a particular measurement, $\mathbf{x}'_{d,j}(t_0)$. This implies a non zero intersection of the two admissible regions, that is,

$$\mathcal{S}_0 \cap Æ_j \neq \emptyset \qquad (48)$$

Fujimoto and Scheeres showed that if two arbitrary admissible region intersect, there is a diminishingly low probability that they were not generated from the same object [29]. This statement implies that whatever orbit in $\mathcal{S}_0$ that could create the measurement $x_{d,j}(t_0)$, are the intersection of these two admissible regions, and therefore the correct orbit. The Fujimoto and Scheeres paper works with exact admissible regions and draws the conclusion that the intersection must necessarily be a single point in the state space. This can be expanded ton include uncertainties in the measurements of $\mathcal{S}_0$ and $Æ_j$, implying a non-point intersection.

$$\mathcal{S}'_0 = \mathcal{S}_0 \cap Æ_j \qquad (49)$$

where $\mathcal{S}'_0$ is a new set of orbits. The new set, $\mathcal{S}'_0$, can also be written as $Æ_i \cap Æ_j$. Note that by definition $\mathcal{S}_0 \supseteq \mathcal{S}_0 \cap Æ_j$, implying that this calculation consists only of deleting parts of $\mathcal{S}_0 = Æ_i$. The knowledge obtained from $\mathbf{x}'_{d,j}(t_0)$ can be used to rate track the object or inform an online matched filter [30].

The problem with this approach is that new measurements can either be significantly noisy or the probability of detection may be below one. In these cases, a sequential Bayesian update scheme, in the form of a particle filter, can be formulated to operate directly on hypothesis test results. At this point, the prior set must be instead thought of as a prior PDF. The uncertainty in $\mathcal{S}_0$ can either be represented by a known prior PDF or with a uniform prior similar to an admissible region.

$$P(\mathbf{x}(t_0)|\mathcal{S}_0) = P(\mathcal{S}_0) \qquad (50)$$

The new measurement defines a Bayesian update

$$P(\mathbf{x}|\mathbf{x}'_{d,j}(t_0)) = \frac{P(\mathbf{x}'_{d,j}(t_0)|\mathbf{x})P(\mathbf{x}|\mathcal{S}_0)}{P(\mathbf{x}'_{d,j}(t_0))} \qquad (51)$$

The measurement likelihood map, $P(\mathbf{x}'_{d,j}(t_0)|\mathbf{x})$, can be calculated from the localization of $x_{d,j}(t_0)$. The localization of $x_{d,j}(t_0)$ must necessarily be calculated from the matched filter result, which is represented by the hypothesis test in Equation (44).

$$P(\mathbf{x}'_{d,j}(t_0)|\mathbf{x}) = P(z_j > 0 \ \forall \ j \in [1, \dots, n]) \qquad (52)$$

The right hand side of Equation (52) is equivalent to the hypothesis test in Equation (44). The matched filter can be built into a Bayesian update, allowing the matched filter bank to be built into a particle-based filter. It should be noted that while this paper's results will only include a basic particle filter, this likelihood can apply to a wide range of filters including random finite set and multi-target filters.

IV. Implementation of Theory

In Figure 7, the logic for an implementation of a matched filter bank based on the work in this paper is mapped out. Boxes 1 and 2 define the prior information for the process. Box 3 maps a prior set of orbits to measurement arcs, which in practice are what is used to partition and generate templates. In Box 5, the pivot point $\mathbf{x}_k$ can be chosen in a few different ways. The simulations in this paper choose the first pivot point randomly and choose all following pivots as the point furthest in MDM from the previous pivot. Box 6 represents comparing the distance between each point and the pivot in MDM. The measurement arcs should be pre-calculated for each point to expedite this. The time density of the measurement arcs should be chosen based on processing power. The partitioning module should pass out both the pivot point and the associated partition set. The subsection labeled "Local Matched Filter" represents how to process the matched filters. $\mathcal{L}$ is the intersection of the measurement frame and a particular partition. In practice, this can be generated by mapping the measurement arcs into the measurement frame with the desired camera model and locating all pixels with any signal. It is useful to pad the localization matrix to expand the search area by a few rows and columns. This assures that if the truth appears near the boundary of the search area, the matched filter correlation peak will be captured fully. If $\mathcal{L}$ is empty, this template can be skipped. If $\mathcal{L}$ is not empty, the non-empty pixels defines the locations where the signal should be checked.

The results should appear similar to Figure 14. The likelihood can be used in a variety of ways: each particle's likelihood can be evaluated for a particle filter update, the peak likelihood can be directly considered as a measurement, or the likelihood itself can used seen as the final product. Another extra processing technique which is worth considering is point spread function (PSF) fitting [31]. This technique involves optimizing over the underlying signal's end points and PSF at sub-pixel accuracy. The matched filter template with the best correlation can be used an initial guess for the PSF fit. The PSF fit result can then be used as the detection, which should lead to sub-pixel accurate localization of endpoints.
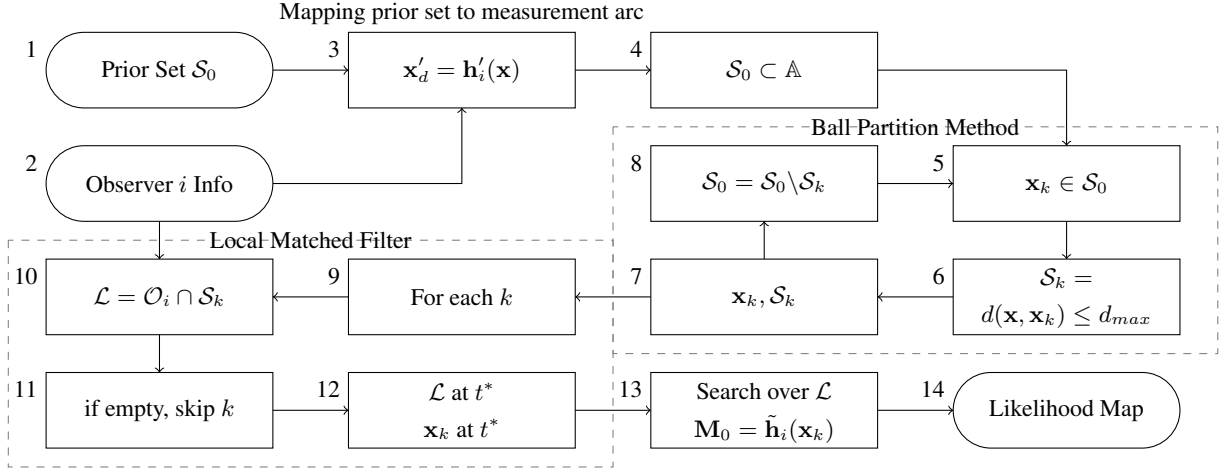
V. Simulation Results

Mapping prior set to measurement arc

Figure 7. Code Flow Diagram for implementing MF Bank

A. Problem Geometry

A medium Earth orbiting object, with parameters in Table 1 is simulated to demonstrate the admissible region hand off. The object is simulated at the following UTC.

a (km)	e	Ω (rad)	i (rad)	ω (rad)	f (rad)
1.2658e+04	0.2198	2.3863	0.3489	1.2698	0.3724

Table 1. orbital elements for simulation

$$UTC = [2011, 11, 12, 20, 34, 07]$$

Two EOS observers, $\mathbf{o}_1$ and $\mathbf{o}_2$, located in Colorado and Hawai'i respectively, take observations of the space object at times $t_1 = 0$s and $t_2 = 120$s. Consider observer 1 to be a high sensitivity sensor able to detect this space object via conventional methods. Consider observer 2 to be a low sensitivity sensor which would normally be unable to detect this space object. The geometry of the problem is shown in Figure 8. The SO and observer position and velocities at the time of the observations are:

$$\mathbf{r}(t_1) = [-5906.3 \quad -7313.5 \quad 3410.0]^T (km)$$
$$\dot{\mathbf{r}}(t_1) = [5.0791 \quad -4.7364 \quad -0.01212]^T (km/s)$$
$$\mathbf{r}(t_2) = [-5280.5 \quad -7860.5 \quad 3398.8]^T (km)$$
$$\dot{\mathbf{r}}(t_2) = [5.3445 \quad -4.3765 \quad -0.17361]^T (km/s)$$
$$\mathbf{o}_1 = [-1207.0 \quad -4746.7 \quad 4072.0]^T (km)$$
$$\dot{\mathbf{o}}_1 = [0.34519 \quad -0.08777 \quad 0.0000]^T (km/s)$$
$$\mathbf{o}_2 = [-5446.2 \quad -2431.8 \quad 2252.0]^T (km)$$
$$\dot{\mathbf{o}}_2 = [0.17337 \quad -0.39759 \quad 0.0]^T (km/s)$$

B. Observations

The first observer takes an image which leads to a detection and measurement by conventional methods. An admissible region is generated from this first observation, seen in Figure 12, as the black outline. The admissible region throughout these simulation results is represented by a discrete point-wise approximation of 20,000 particles. The second observer, $\mathbf{o}_2$, takes low SNR observation of the SO, also at $t_2 = 120$s. The image can be seen in Figure 13. The image simulation is done without star signals, to prevent false detections. Stars will present a problem in implementation on real data, but can be avoided with good star identification and subtraction. The image is generated with a 10 second exposure time, field of view of 10 degrees, and sidereal stare
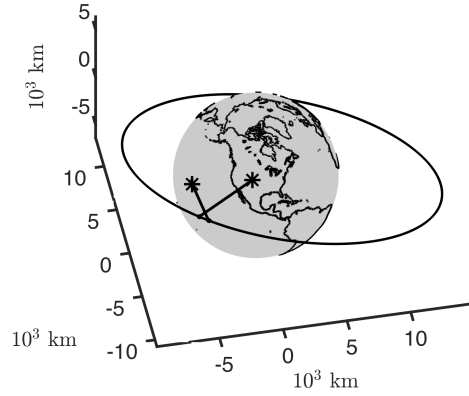

Figure 8. Location of Observers and SO

pointing mode. The total object SNR in this image is approximately 6.8, while the maximum pixel-wise SNR in this image is approximately 1.0. Conventional methods, such as thresholding and corner detection, fail to detect this object. Because the only orbital knowledge on this object in the admissible region from observer 1, conventional velocity filters cannot be implemented.

C. Partitioning

In order to give insight into the computational cost of the ball partitioning, the simulation has been run for a range of MDM threshold values. For these multi-value test runs, object SNR is set to approximately 0.25, the probability of false alarm threshold is set to 0.999, and 10,000 particles are used to represent the AR. In Figure 9, the maximum likelihood is shown to vary more significantly with a higher MDM threshold. Because raw measurement SNR is constant, a perfect template should always provide the same Likelihood. The sporadic behavior at high MDM threshold is a result of the inability of a high MDM threshold to consistently provide effective templates. The number of templates and computation time are plotted against MDM Threshold on a log-log scale in Figure 10. Computation time follows a predictable curve; more templates proportionately leads to more computation time.

Next, a particular partitioning will be shown in more detail. In remaining simulations, object SNR is set to approximately 1, the probability of false alarm threshold is set to 0.999, and 20,000 particles are used to represent the AR. A maximum MDM value of $d_{max} = 0.1 \ rad \cdot s$ is chosen. The measurement arc is calculated for each particle, represented by a time series of unit vectors. A ball partitioning
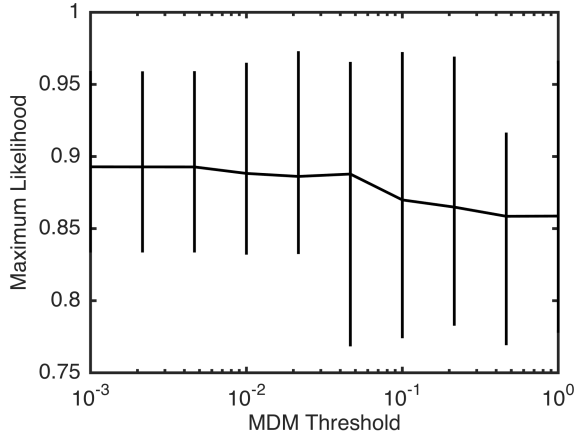
algorithm based on approximate integration over the time series sorts the particles into subsets containing consistent orbits. The partitioning provides 80 distinct partitions with corresponding templates. Figure 11 shows a sample of the types of templates which are generated. Figure 12 shows the partitions on the original admissible region. Three particular partitions, labeled A, B, and C, will be followed more closely through the remaining process.

Figure 11. Sampling of matched filter templates from partitioning.

Figure 9. Maximum Likelihood results from varying MDM threshold.
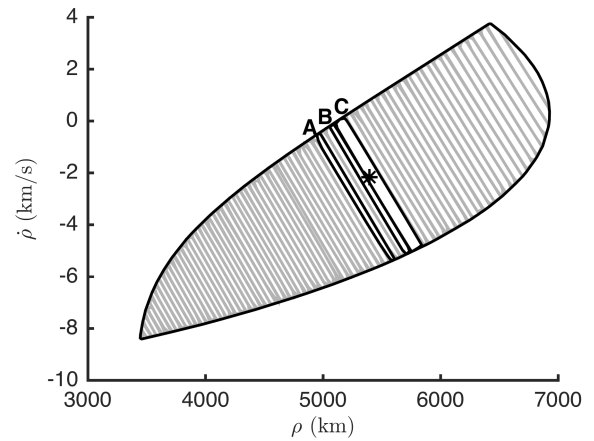
Figure 12. Sets generated from partitioning, shown on original AR.

D.   Observation Search

The templates with corresponding partitions are searched in the image. The matched filter gives a value for each pixel in the image which the template is centered at. Each matched filter result is then tested via the hypothesis test in Equation (44). This gives a likelihood function over the partition, which can evaluated for all particles. Figure 14 shows the correlation maps for three templates. Figure 14a shows an incorrect template which doesn't produce significant SNR gain. Figure 14b shows a template with an imperfect template, illustrating the kind of SNR gain possible in real operation. Figure 14c shows a template primed with perfect orbital knowledge, simply to illustrate what the ideal case can look like.

E.   Orbit Update

The final step is calculate a Bayesian update on the space object. Each particle's likelihood is evaluated within its partition. Some particles do not fall within the EOS image which poses a problem for the update. These results chose to leave the statistic weights constant on all objects without an available likelihood update. Using the new measurements, the PDF over the original admissible region can be updated, point-wise, similar to a particle filter update. Figure 15 shows the results of the Bayesian update. It is important to note that this method does not make a hard update decision and shouldn't. Ultimately, this would be used in a filtering scheme such as a particle filter or multiple hypothesis filter, as the likelihood function.

F.   Sequential Particle Filter

As of now, the likelihood function update at a given time only makes sense if it can be evaluated for all objects within the PDF. The fol-
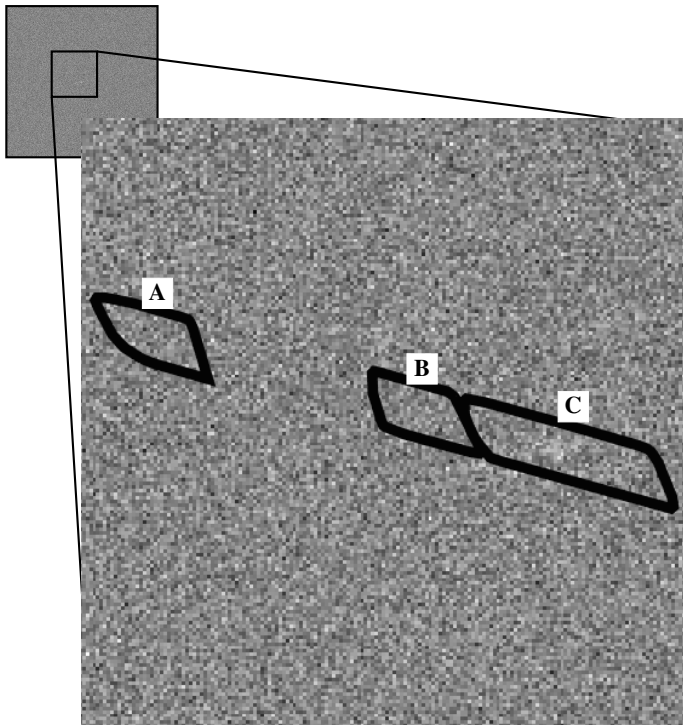

Figure 10. Computational time results from varying MDM threshold.

Figure 13. Measurement Image taken by observer 2
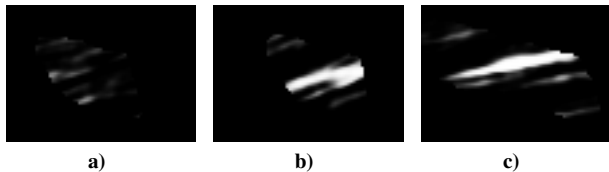

| a) | b) | c) |

Figure 14. Correlation results from a variety of templates
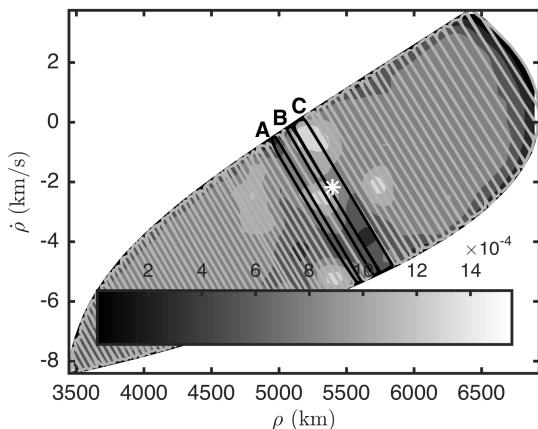

Figure 15. Final PDF update from matched filter likelihood.

lowing results will proceed under the assumption that the measurement likelihood can be evaluated for all particles. Two observers in Georgia and a MEO object are simulated. Similar to the previous simulation, the first observer takes an observation of the object and an admissible region is created. The AR is passed off to the second observer, which then takes a series of 9 observations. Each observation is a 10 second exposure, sidereal stare observation, which are initiated at 20 second intervals. The following initial parameters are used

$$\mathbf{r}(t_1) = [-3420.2 \quad -8138.0 \quad 4698.5]^T (km)$$
$$\dot{\mathbf{r}}(t_1) = [6.5260 \quad -2.3753 \quad -0.0121]^T (km/s)$$
$$\mathbf{o}_1 = [652.95 \quad -5284.4 \quad 3499.5]^T (km)$$
$$\dot{\mathbf{o}}_1 = [0.3843 \quad 0.0475 \quad 0.0000]^T (km/s)$$
$$\mathbf{o}_2 = [522.51 \quad -5281.8 \quad 3525.1]^T (km)$$
$$\dot{\mathbf{o}}_2 = [0.3841 \quad 0.0380 \quad 0.0]^T (km/s)$$

The final posterior PDF of the particle filter can be seen in Figure 16. The standard deviations in range and range rate space can be seen plotted over iterations in Figure 17. The final values of the particle filter are highly dependent on factors such as process noise, image pixel size, object SNR, and more. These plots are meant to demonstrate that particle filter convergence is possible. Object SNR over the series of images is shown in Figures 18 and 19. Figure 18 shows the total object SNR calculated by Equation (7). The total object SNR, which is the SNR of all pixels which the object appears in, gives an idea of the total available information for an object. Figure 18 shows the maximum per pixel SNR calculated by Equation (5). The maximum per pixel SNR gives a measure of the ability of classical detection methods (thresholding, edge detection) to detect this object. It is worth noting that this particle filter scales gracefully for different object SNR values. This means that this method can be used as a general object detection method which can capture dim space objects.
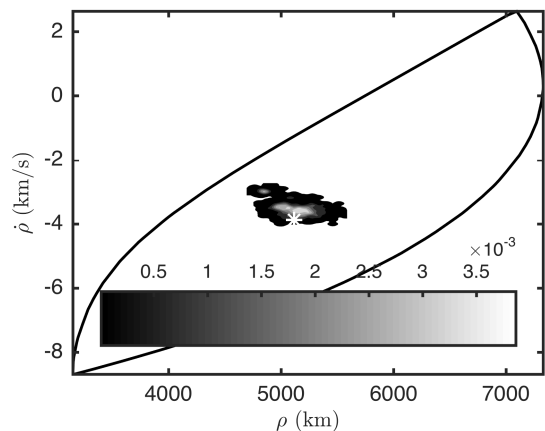

Figure 16. Final PDF update from multi-frame matched filter likelihood particle filter.

VI.   Conclusion

A methodology has been developed for obtaining low SNR detections of space objects when uncertain prior information is available. Unlike typical matched filters, exact knowledge is not necessary with this matched filter bank. The partitioning method that is proposed in this paper enables efficient and mathematically rigorous generation of the matched filter bank. A novel metric is first defined in this paper, upon which the partition process is defined. The resulting partitions are then used for an analytic result which allows the localization of a matched filter. This MF bank enables a statistical update to an orbit to be derived directly from image data. Reliable low SNR detection methods have the ability to decrease require costs for performing SDA with
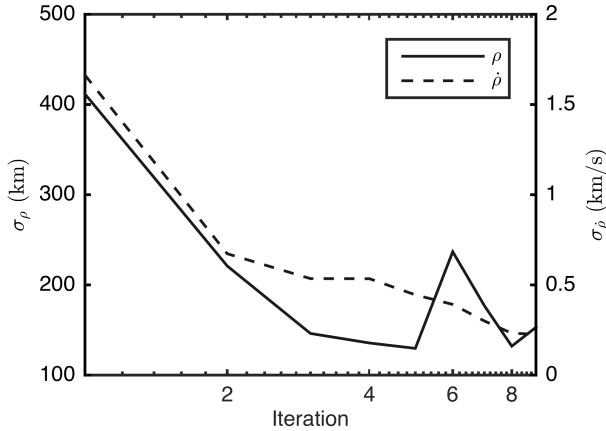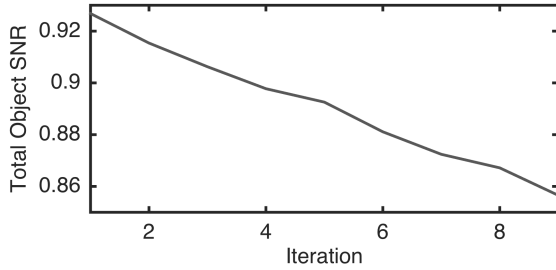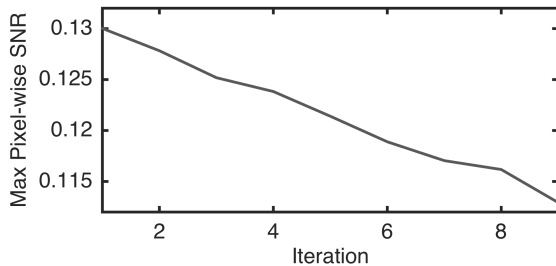
electro-optical sensors. Instead of building more monolithic telescopes, large numbers of smaller sensors can be used to gather important SDA data. Large, exquisite sensors can then be focused on object discovery rather than catalog upkeep. Furthermore, this methodology can be generalized to a wide variety of sensors and data types.

Appendix: VI

A typical optical measurement of a space object contains good knowledge of angle and angle rates known as observable states, $\mathbf{x}_d \in \mathbb{R}^4$. An orbit requires six disparate data types to be fully constrained. Historically, the final two data types are angle accelerations or range and range rate (from radar data). This AR formulation uses range and range rate as the final two states, known as undetermined states $\mathbf{x}_u \in \mathbb{R}^2$. It is assumed that no information can be reliably used to determine these states from measurements. The following notation was developed by Worthy et al [32]. Using equations (9) and (11) and the fact that the measurement cannot be dependent on $\mathbf{x}_u$, the following measurement function can be written.

$$\mathbf{y}(t) = \mathbf{h}(\mathbf{x}_d; \mathbf{k}, t) \tag{53}$$

Furthermore, this implies a one to one and onto relationship between $\mathbf{y}(t)$ and $\mathbf{x}_d$

$$\mathbf{x}_d = \mathbf{h}^{-1}(\mathbf{y}; \mathbf{k}, t) \tag{54}$$

An AR is then created by enforcing a series of constraints of the form

$$g_i(\mathbf{x}_d, \mathbf{x}_u; \mathbf{k}, t) \leq 0 \tag{55}$$

$$g_i(\mathbf{h}^{-1}(\mathbf{y}; \mathbf{k}, t), \mathbf{x}_u; \mathbf{k}, t) \leq 0 \tag{56}$$

It should be noted that these constraints can be thought of as hypotheses. The AR is then the space where all hypotheses are true. Next, we define an admissible region, $\mathcal{AR}_i \in \mathbb{R}^2$, predicated on g_i

$$\mathcal{AR}_i := \left\{ \mathbf{x}_u | g_i(\mathbf{h}^{-1}(\mathbf{y}; \mathbf{k}, t), \mathbf{x}_u; k, t) \leq 0 \right\} \tag{57}$$

In practice, an admissible region predicated on n constraints is used.

$$\mathcal{AR} = \bigcap_{i=1}^{n} \mathcal{AR}_i \tag{58}$$

Next, the two most common constraints are defined. For optical observer AR, the primary constraint typically considered is that of Earth-orbiting SO, defined as $g_{\mathcal{E}}$. There exists a derivation to show the following equations represent energy as a function of $[\rho, \dot{\rho}]$ and known parameters. The following results were originally derived for Earth objects by Tommei et al [33]. $\mathcal{E}$ is the orbital energy, which must be negative for an Earth-orbiting SO.

$$2\mathcal{E} = g_{\mathcal{E}}(\mathbf{h}^{-1}(\mathbf{y}; \mathbf{k}, t), \mathbf{x}_u; \mathbf{k}, t) \leq 0 \tag{59}$$

$$2\mathcal{E} = \dot{\rho}^2 + w_1\dot{\rho} + T(\rho) - \frac{2\mu}{\sqrt{S(\rho)}} \leq 0 \tag{60}$$

$$T(\rho) = w_2\rho^2 + w_3\rho w_4 \tag{61}$$

$$S(\rho) = \rho^2 + w_5\rho + w_0 \tag{62}$$

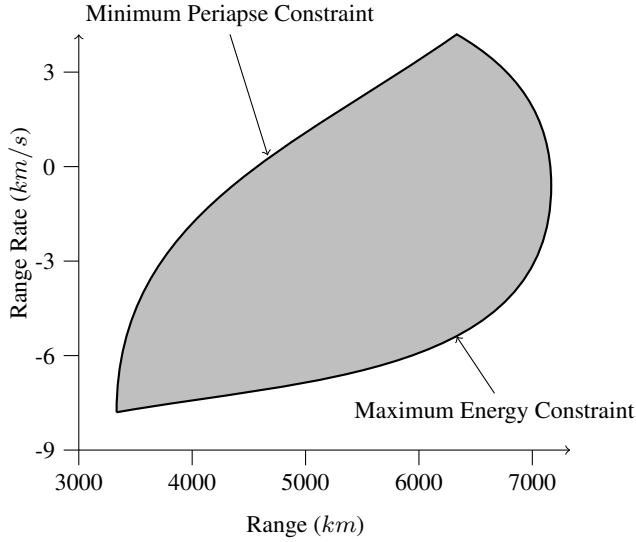where the constants w_{0-5} are functions of the parameter vector, $\mathbf{k}$, defined as

Figure 17. Standard Deviation of PF over iterations.

Figure 18. Object SNR over observation series.

Figure 19. Object SNR over observation series.

Figure 20. Sample admissible region

References

[1] Rossi, A., "The earth orbiting space debris," *Serbian Astronomical Journal*, Vol. 170, No. 1, 2005, pp. 1–12.

[2] Kelso, T. et al., "Analysis of the iridium 33 cosmos 2251 collision," Tech. rep., Center for Space Standards & Innovation, 2009.

[3] Liou, J., "Modeling the Large and Small Orbital Debris Populations for Environment Remediation," 2013.

[4] Morales, M. D., "Space Fence program awards contracts for concept development," July 2009.

[5] Coder, R. D. and Holzinger, M. J., "Multi-Objective Design of Optical Systems for Space Situational Awareness," *Advances in Space Research*, 2015, submitted.

[6] Levesque, M., "Automatic reacquisition of satellite positions by detecting their expected streaks in astronomical images," *Proceedings of the Advanced Maui Optical and Space Surveillance Technologies Conference*, 2009, p. E81.

[7] North, D. O., "An analysis of the factors which determine signal/noise discrimination in pulsed-carrier systems," *Proceedings of the IEEE*, Vol. 51, No. 7, 1963, pp. 1016–1027.

[8] Mohanty, N., "Computer tracking of moving point targets in space," *Pattern Analysis and Machine Intelligence, IEEE Transactions on*, , No. 5, 1981, pp. 606–611.

[9] Reed, I., Gagliardi, R., and Shao, H., "Application of three-dimensional filtering to moving target detection," *Aerospace and Electronic Systems, IEEE Transactions on*, Vol. AES-19, No. 6, 1983, pp. 898–905.

[10] Dragovic, M., "Velocity filtering for target detection and track initiation," Tech. rep., DTIC Document, 2003.

[11] Milani, A., Gronchi, G. F., Vitturi, M. d., and Knežević, Z., "Orbit determination with very short arcs. I admissible regions," *Celestial Mechanics and Dynamical Astronomy*, Vol. 90, No. 1-2, 2004, pp. 57–85.

[12] Farnocchia, D., Tommei, G., Milani, A., and Rossi, A., "Innovative methods of correlation and orbit determination for space debris," *Celestial Mechanics and Dynamical Astronomy*, Vol. 107, No. 1-2, 2010, pp. 169–185.

[13] DeMars, K. J. and Jah, M. K., "Probabilistic initial orbit determination using gaussian mixture models," *Journal of Guidance, Control, and Dynamics*, Vol. 36, No. 5, 2013, pp. 1324–1335.

[14] Zingarelli, J. C., Pearce, E., Lambour, R., Blake, T., Peterson, C. J., and Cain, S., "Improving the Space Surveillance Telescope's Performance Using Multi-Hypothesis Testing," *The Astronomical Journal*, Vol. 147, No. 5, 2014, pp. 122.

[15] Mahler, R. P., *Statistical multisource-multitarget information fusion*, Artech House, Inc., 2007.

[16] Blackman, S., "Multiple Hypothesis Tracking For Multiple Target Tracking," *IEEE A and E Systems Magazine*, 2004.

[17] Tonissen, S. and Evans, R., "Peformance of dynamic programming techniques for Track-Before-Detect," *IEEE Trans. Aerosp. Electron. Syst.*, Vol. 32, No. 4, 1996, pp. 1440–1451.

[18] Zhai, C., Shao, M., Nemati, B., Werne, T., Zhou, H., Turyshev, S. G., Sandhu, J., Hallinan, G., and Harding, L. K., "DETECTION OF A FAINT FAST-MOVING NEAR-EARTH ASTEROID USING THE SYNTHETIC TRACKING TECHNIQUE," *ApJ*, Vol. 792, No. 1, aug 2014, pp. 60.

[19] Zezula, P., Amato, G., Dohnal, V., and Batko, M., *Similarity search: the metric space approach*, Vol. 32, Springer Science & Business Media, 2006.

$$w_0 = ||\mathbf{o}||^2 \tag{63}$$
$$w_1 = 2\dot{\mathbf{o}} \cdot \hat{\boldsymbol{\rho}} \tag{64}$$
$$w_2 = \dot{\alpha}^2 \cos^2 \delta + \dot{\delta} \tag{65}$$
$$w_3 = 2(\dot{\alpha}\dot{\mathbf{o}} \cdot \hat{\boldsymbol{\rho}}_\alpha + \dot{\delta}\dot{\mathbf{o}} \cdot \hat{\boldsymbol{\rho}}_\delta) \tag{66}$$
$$w_4 = ||\dot{\mathbf{o}}||^2 \tag{67}$$
$$w_5 = 2\mathbf{o} \cdot \hat{\boldsymbol{\rho}} \tag{68}$$

where $\mathbf{o}$ and $\dot{\mathbf{o}}$ are the position and velocity of the observer, $\hat{\boldsymbol{\rho}}$ is the unit vector from the angles, and $\hat{\boldsymbol{\rho}}_\alpha$ and $\hat{\boldsymbol{\rho}}_\delta$ are given by

$$\hat{\boldsymbol{\rho}} = [\cos\alpha\cos\delta \quad \sin\alpha\cos\delta \quad \sin\delta]^T \tag{69}$$
$$\hat{\boldsymbol{\rho}}_\alpha = [-\sin\alpha\cos\delta \quad \cos\alpha\cos\delta \quad 0]^T \tag{70}$$
$$\hat{\boldsymbol{\rho}}_\delta = [-\cos\alpha\sin\delta \quad -\sin\alpha\sin\delta \quad \cos\delta]^T \tag{71}$$

A second commonly used constraint is g_r, a constraint on the radius of perigee. There exists a analytic derivation for the following [12]. It should be noted that $\mathbf{D}$, $\mathbf{E}$, $\mathbf{F}$, and $\mathbf{G}$ are vector quantities.

$$g_r(\rho, \dot{\rho}, \mathbf{x}_d; \mathbf{k}) = (r_{min}^2 - ||\mathbf{D}||^2)\dot{\rho} - P(\rho)\dot{\rho} - U(\rho) + r_{min}^2 T(\rho) - \frac{2r_{min}\mu}{\sqrt{S(\rho)}} \tag{72}$$

$$P(\rho) = 2\mathbf{D} \cdot \mathbf{E}\rho^2 + 2\mathbf{D} \cdot \mathbf{F}\rho + 2\mathbf{D} \cdot \mathbf{G} - r_{min}^2 w_1 \tag{73}$$

$$U(\rho) = ||\mathbf{E}||^2\rho^4 + 2\mathbf{E} \cdot \mathbf{F}\rho^3 + (2\mathbf{E} \cdot \mathbf{G} + ||\mathbf{F}||^2)\rho^2 + 2\mathbf{F} \cdot \mathbf{G}\rho + ||\mathbf{G}||^2 - 2r_{min}\mu \tag{74}$$

where the $\mathbf{D}$, $\mathbf{E}$, $\mathbf{F}$, and $\mathbf{G}$ are defined as

$$\mathbf{D} = \mathbf{q} \times \hat{\boldsymbol{\rho}} \tag{75}$$
$$\mathbf{E} = \hat{\boldsymbol{\rho}} \times (\dot{\alpha}\hat{\boldsymbol{\rho}}_\alpha + \dot{\delta}\hat{\boldsymbol{\rho}}_\delta) \tag{76}$$
$$\mathbf{F} = \mathbf{q} \times (\dot{\alpha}\hat{\boldsymbol{\rho}}_\alpha + \dot{\delta}\hat{\boldsymbol{\rho}}_\delta) + \hat{\boldsymbol{\rho}} \times \dot{\mathbf{q}} \tag{77}$$
$$\mathbf{G} = \mathbf{q} \times \dot{\mathbf{q}} \tag{78}$$

More ways exist to further constrain an admissible region. Beyond perigee and energy, any further restriction typically requires an assumption about the object. For example, if the object being observed is known to be near a GEO, constraints could be placed on semi major axis or eccentricity. This can enable prior orbital knowledge to be used to enhance convergence.

[20] Benezeth, Y., Jodoin, P., Emile, B., Laurent, H., and Rosenberger, C., "Review and evaluation of commonly-implemented background subtraction algorithms," *2008 19th International Conference on Pattern Recognition*, Institute of Electrical & Electronics Engineers (IEEE), dec 2008.

[21] Pratt, W. K., *Digital Image Processing*, Wiley-Blackwell, jan 2007.

[22] Turin, G. L., "An introduction to matched filters," *IRE Transactions on Information Theory*, Vol. 6, No. 3, jun 1960, pp. 311–329.

[23] Chávez, E., Navarro, G., Baeza-Yates, R., and Marroquín, J. L., "Searching in metric spaces," *ACM computing surveys (CSUR)*, Vol. 33, No. 3, 2001, pp. 273–321.

[24] Uhlmann, J. K., "Satisfying general proximity/similarity queries with metric trees," *Information processing letters*, Vol. 40, No. 4, 1991, pp. 175–179.

[25] Batko, M., Novak, D., and Zezula, P., "MESSIF: Metric Similarity Search Implementation Framework," *Digital Libraries: Research and Development*, Springer Science, Business Media, 2007, pp. 1–10.

[26] Gionis, A., Indyk, P., Motwani, R., et al., "Similarity search in high dimensions via hashing," *VLDB*, Vol. 99, 1999, pp. 518–529.

[27] Montgomery, D. C. and Runger, G. C., *Applied statistics and probability for engineers*, John Wiley & Sons, 2010.

[28] Sease, B., Schmittle, K., and Flewelling, B., "MULTI-OBSERVER RESIDENT SPACE OBJECT DISCRIMINATION AND RANGING," *AAS/AIAA Space Flight Mechanics Meeting*, 2015.

[29] Fujimoto, K. and Scheeres, D. J., "Applications of the admissible region to space-based observations," *Advances in Space Research*, Vol. 52, No. 4, 2013, pp. 696–704.

[30] Sease, B., Murphy, T., Flewelling, B., Holzinger, M. J., and Black, J., "Enabling direct feedback between initial orbit determination and sensor data processing for detection and tracking of space objects," *SPIE Defense+ Security*, International Society for Optics and Photonics, 2015, pp. 94690M–94690M.

[31] Kouprianov, V., "Distinguishing features of CCD astrometry of faint GEO objects," *Advances in Space Research*, Vol. 41, No. 7, 2008, pp. 1029–1038.

[32] Worthy III, J. L. and Holzinger, M. J., "Incorporating Uncertainty in Admissible Regions for Uncorrelated Detections," *Journal of Guidance, Control, and Dynamics*, Vol. 0, No. 0, 2015, pp. 1–17.

[33] Tommei, G., Milani, A., and Rossi, A., "Orbit determination of space debris: admissible regions," *Celestial Mechanics and Dynamical Astronomy*, Vol. 97, No. 4, 2007, pp. 289–304.